QM/MM-MD Simulations of Conjugated Polyelectrolytes: A Study on Luminescent Conjugated Oligothiophenes for Use as Bio-Physical Probes.

ARTICLE *in* THE JOURNAL OF PHYSICAL CHEMISTRY A · APRIL 2014

Impact Factor: 2.69 · DOI: 10.1021/jp5009835 · Source: PubMed

THE JOURNAL OF PHYSICAL CHEMISTRY A

Article

pubs.acs.org/JPCA

QM/MM-MD Simulations of Conjugated Polyelectrolytes: A Study of Luminescent Conjugated Oligothiophenes for Use as Biophysical Probes

Jonas Sjöqvist,[†] Mathieu Linares,[†] Kurt V. Mikkelsen,[‡] and Patrick Norman*[,†]

[†]Department of Physics, Chemistry and Biology, Linköping University, SE-581 83 Linköping, Sweden

[‡]Department of Chemistry, University of Copenhagen, Universitetsparken 5, DK-2100 Copenhagen Ø, Denmark

Supporting Information

ABSTRACT: A methodological development is reported for the study of luminescence properties of conjugated polyelectrolytes, encompassing systems in which dihedral rotational barriers are easily overcome at room temperature. The components of the model include (i) a molecular mechanics (MM) force field description of the solvent in its electronic ground state as well as the chromophore in its electronic ground and excited states, (ii) a conformational sampling by means of classical molecular dynamics (MD) in the respective electronic states, and (iii) spectral response calculations by means of the quantum mechanics/molecular mechanics QM/MM approach. A detailed analysis of the combined polarization effects of the ionic moiety and the polar water solvent is presented. At an increased computational cost of 30% compared to a calculation excluding the solvent, the error in the transition wavelength of the dominant absorption band is kept as small as 1 nm as compared to the high-quality benchmark result, based largely on a QM description of the solvent. At a *reduced* computational cost the error of the same quantity is kept as small as 6 nm, with the cost reduction being the result of an effective description of the effects of the solvent by means of replacing the carboxylate ions with neutral hydrogens. In absorption spectroscopy, the obtained best theoretical results are in excellent agreement with the experimental benchmark measurement, regarding excitation energies as well as band intensities and profiles. In fluorescence spectroscopy, the experimental spectrum shows a vibrational progression that is not addressed by theory, but the theoretical band position is in excellent agreement with experiment, with a highly accurate description of the Stokes shift as a result.

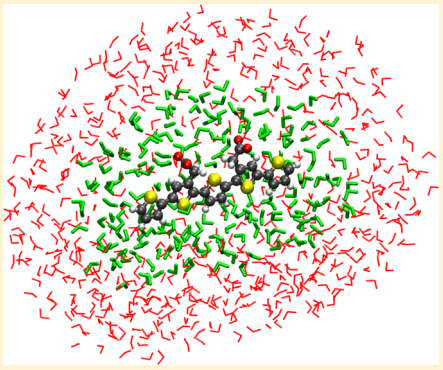

I. INTRODUCTION

Fluorescence probes are an important tool in biomedical applications, allowing detection of cells and proteins connected to a number of diseases, including Alzheimer's disease[1−11] and different cancers.[12−20] Traditionally, the probes used are small fluorophores, fluorescent proteins,[21] or quantum dots,[22,23] but, for each of these classes, limitations exist that make them less than ideal for bioimaging purposes. Small fluorophores and fluorescent proteins usually exhibit low photobleaching thresholds,[22,24] where the light causing the probe to fluoresce also destroys its functionality, disallowing three-dimensional (3D) imaging as well as imaging over longer time scales. Quantum dots do not suffer from this problem but can instead be toxic due to the inclusion of heavy metals such as cadmium, which restricts the possibilities for *in vivo* studies.[22,23] These limitations in standard fluorescence probes have spurred a search for alternative materials.

Conjugated polyelectrolytes[25−28] (CPEs) represent an alternative class of molecules that has shown great promise, not just in the field of bioimaging but also for use in solar cells[27,29,30] and organic light emitting diodes.[27,28] CPEs are polymers (or oligomers) formed by a conjugated backbone together with ionic side chains that make the systems water-soluble. The optical properties of the neutral conjugated polymers are very much preserved in the CPEs,[31−33] and they can thus be tailored through backbone synthetic alterations. This, combined with a high photobleaching threshold and low cytotoxicity, makes them well suited for use in bioimaging applications, where they have been used to study misfolded proteins, connected to such diseases as Alzheimer's disease and type II diabetes,[1] as well as for cancer cell imaging.[16−20]

With the intense experimental interest in CPEs comes an increased need for a microscopic understanding of basic intermolecular interactions and their influence on the optical properties of the probes. Alongside the experimental activities of Nilsson and co-workers, we have undertaken a long-term theoretical study of a group of CPEs known as luminescent conjugated oligothiophenes (LCOs)[1,34−37] that are used as molecular dyes for the detection and characterization of amyloid proteins. As a main result of our first study,[38] we

Received: January 28, 2014
Revised: April 16, 2014
Published: April 16, 2014

presented a set of accurate molecular mechanics (MM) force field parameters for the electronic ground and excited states involved in the fluorescence process, and, by means of a combination of classical molecular dynamics (MD) and quantum chemical response theory, we obtained absorption and fluorescence spectra at room temperature. These calculations included the indirect effects of the aqueous environment in terms of its effect on the molecular dynamics, but they neglected any direct polarization effects on the electronic responses. This is clearly a questionable approximation for charged species, such as polyelectrolytes, and the aim of the present work is to address this specific issue. We will quantify the polarization effects of the ionic groups and the water solvent on the conjugated backbone of the CPEs. In addition to adopting a quantum mechanical (QM) description of the water solvent, we will also employ nonpolarizable and polarizable force fields in a quantum mechanical/molecular mechanical (QM/MM) framework combined with molecular dynamics simulations. Our intention is to investigate how to combine QM/MM-MD calculations with an efficient computational procedure of how to include specific and bulk solvation effects, along with the effects of ionic charges. The appearance of ionic charges in the QM/MM-MD calculations is expected to significantly alter previous procedures for obtaining solvent effects on excitation energies and other molecular properties. Our MM-MD calculations are concerned with not only the electronic ground state but also the excited state so that absorption/excitation and fluorescence spectroscopies are both addressed in the QM/MM-MD framework, and accurate estimates of the Stokes shift are obtained as a result. In fluorescence mode, our approach accounts for the equilibration of the nuclear motions (slow response) but not the electronic polarization (fast response) of the solvent, as the latter would require the optimization of the excited state electron density.

A quantitatively accurate, yet computationally inexpensive, model for studies of optical properties of CPEs will be presented, and, since this study is performed for a prototypical conjugated polyelectrolyte in an aqueous environment, our findings should carry broad interest. To the best of our knowledge, earlier designs of solvation models do not include this important class of systems in the context of bioimaging, and the present work will serve as a platform for our continued work on LCOs.

II. METHODOLOGICAL APPROACH

A. Solvation Methods. Inclusion of the polarization effects of the solvent in the response theory part of the calculations can be achieved by describing the solute and the solvent at different levels of theory, either by way of a continuum or a discrete model. In continuum models,[39−42] a cavity is formed around the solute, and the outside is represented by a dielectric medium. This approach gives an averaged description of the solute interaction which is computationally efficient but incapable of dealing with solvent effects where the discrete nature of the solvent plays a role. These discrete interactions are better dealt with by solvent models such as the QM/MM methods,[42−50] where the individual molecules of the solvent are described by classical force fields. The drawback here is that some form of averaging of the solvent distribution around the solute is required. This can be done either by creating an average of the desired property from many calculations performed for snapshots taken from an MD simulation[48,51−54] or single calculations performed for averaged structures[55] or solvent potentials.[56] We will adopt an averaging based on samples taken from MD trajectories in combination with QM/MM calculations of electronic responses.

B. QM/MM. In QM/MM theory, the Hamiltonian is given by[42−50]

$$\hat{H} = \hat{H}_{QM} + \hat{H}_{QM/MM} + \hat{H}_{MM} \quad (1)$$

where $\hat{H}_{QM}$ is the Hamiltonian of the isolated QM system, $\hat{H}_{QM/MM}$ is the coupling between the QM and MM regions, and $\hat{H}_{MM}$ is the potential energy function of the force field. In this work, each molecule as a whole belongs to either the QM or the MM region, relieving us from the consideration of bond cleavage, and atoms in the MM region are described by point charges and isotropic polarizabilities. When this is the case, the coupling Hamiltonian is given by

$$\hat{H}_{QM/MM} = \hat{H}_{vdw} + \hat{H}_{el} + \hat{H}_{pol} \quad (2)$$

The first term, $\hat{H}_{vdw}$, is calculated entirely classically. A van der Waals parameter is assigned to each atomic nucleus of the QM region, and the interaction energy between the atoms of the QM and MM regions is calculated using the van der Waals function of the force field, in our case a 6-12 Lennard-Jones potential. Since this term does not depend on the electronic coordinates, it will not contribute to electronic response properties. The second term, $\hat{H}_{el}$, represents the electrostatic interaction between nuclei and electrons in the QM region and point charges in the MM region. While the interaction between nuclei and point charges is constant, the interaction between electrons and point charges depends on the form of the wave function and will have a direct effect on the response calculation. The third term in the coupling Hamiltonian, $\hat{H}_{pol}$, includes the interaction between the charges of the QM region and the total induced dipole moments of the MM region as well as the interaction between the parts of the induced dipole moments within the MM region that are caused by the QM region.

The computational cost associated with the van der Waals and electrostatic terms is small relative to that for the QM part, so adding nonpolarizable MM regions to the system is computationally inexpensive. This need not be true, however, for the interaction between the induced dipoles in the MM region and the electron density in the QM region, due to their interdependency, meaning that the solution must be found in an iterative and self-consistent field manner.

C. Solvation Study. We performed a study on one of the LCOs called *p*-HTAA, shown in Figure 1, to find a model that not only allows the inclusion of solvent effects but also has a low enough computational scaling to allow for hundreds of snapshot calculations. The study was carried out by systematically increasing the quality of the description of the water surrounding a single snapshot of *p*-HTAA, taken from a room temperature molecular dynamics simulation. This was done by dividing the surrounding solvent into regions described at different levels of theory and then calculating the linear absorption spectrum of the system using QM/MM response theory[47,48,55,57,58] while varying the sizes of the regions. On the basis of these calculations, the excitation energy and oscillator strength of the dominant excited state were compared and taken as the measure of the quality of the model.

Three levels of theory were used: a QM description closest to the solute, a polarizable MM model outside of that, and finally a nonpolarizable MM model. The regions were defined

dx.doi.org/10.1021/jp5009835 | J. Phys. Chem. A 2014, 118, 3419−3428

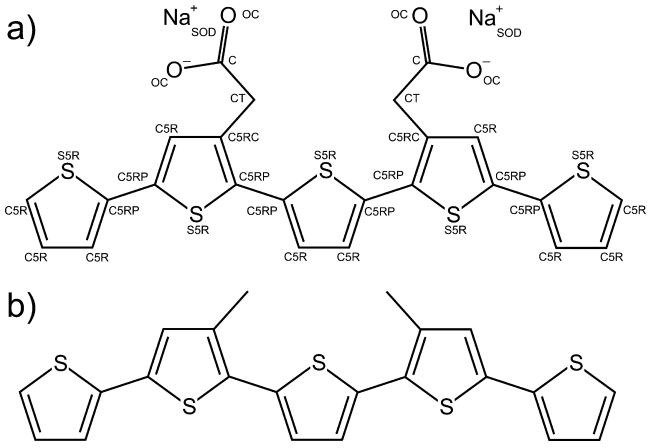

Figure 1. Molecular structures of (a) the full *p*-HTAA chromophore, along with CHARMM atom type definitions, and (b) the cut-down model.

as shells around the solute, based on the distance between the oxygen atoms of the water molecules and the nearest atom of the solute. Starting from a completely unsolvated system, the nonpolarizable MM region was increased by steps of 1 Å until a maximum thickness of 15 Å was reached. This process was repeated for the polarizable MM region. In addition, starting from a 15 Å thick layer of nonpolarizable water, the size of the polarizable MM region was increased by 1 Å at a time until it had replaced all the nonpolarizable water. An example of this is shown in Figure 2, where the *p*-HTAA chromophore is surrounded by two shells of thicknesses 7 and 8 Å, respectively.

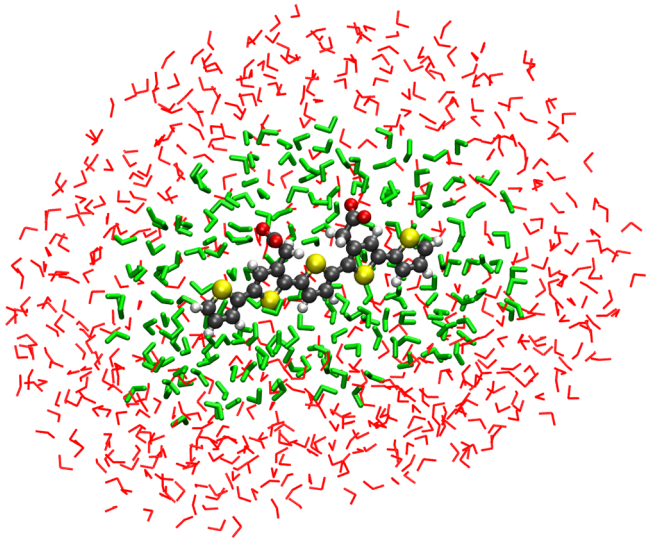

Figure 2. The *p*-HTAA chromophore surrounded by 7 Å (green) and 8 Å (red) thick layers of polarizable and nonpolarizable water, respectively.

A benchmark was obtained by considering a 4 Å thick layer of QM water surrounded by an 11 Å thick layer of polarizable MM water. These solvation shells contained 63 and 1067 water molecules, respectively. Molecules outside a radius of 15 Å were neglected.

D. Molecular Mechanics. In our previous work, a set of CHARMM force field parameters were derived to describe the LCO class of chromophores. The parametrization was based on a set of rudimentary parameters found in the CHARMM22 set and focused on the bonds connecting the thiophene rings as well as the torsional barriers between them. In this work, a further refinement was made to the parameters, this time focused on the structural parameters of the thiophene rings.

In the CHARMM force field, both the bond stretching and angle bending interactions are described by harmonic oscillators as

$$E_b = K_b(b - b_0)^2 \tag{3}$$

and

$$E_\theta = K_\theta(\theta - \theta_0)^2 \tag{4}$$

where b is the distance between two bonded atoms, θ is an angle formed by two atoms bonded to a common third atom, K_b and K_θ are force constants, and b_0 and θ_0 are equilibrium distances and angles, respectively. In this work, a number of equilibrium parameters from the CHARMM22 parametrization have been altered, while keeping the original force parameters.

E. Averaged Absorption Spectra. The dyes studied in this work are composed of highly flexible chains of thiophene rings that rotate quite freely at room temperature.[59] To account for this flexibility in the spectrum calculations, a method of conformational averaging is employed, combining classical molecular dynamics simulations with quantum chemical response theory calculations. In this method, a large number of uncorrelated structural snapshots are sampled from an MD simulation, and a response theory spectrum calculation is performed for each. The final spectrum is obtained as an average of all the single spectra. The method used follows the approach described in refs 47, 48, and 60.

The expression used for obtaining an averaged absorption spectrum, from the ground state $|0\rangle$ to the excited state $|n\rangle$, or an averaged fluorescence spectrum, from the excited state $|n\rangle$ to the ground state $|0\rangle$, is the following

$$\sigma^{n\leftrightarrow 0}(\omega) \approx \frac{1}{N}\sum_{i=1}^{N} \Delta\omega_0^n(R_i)|\mu(R_i)|^2 g[\omega - \Delta\omega_0^n(R_i)] \tag{5}$$

where the index i denotes samples taken from an MD trajectory in the ground state $|0\rangle$ or excited state $|n\rangle$, respectively, and R_i are the nuclear coordinates of that sample. The vertical electronic transition frequency of the sample is denoted by $\Delta\omega_0^n(R_i)$, and the corresponding electric transition dipole vector is given by $\mu(R_i)$. The function g is a line-shape function.

In this work, the spectrum calculations are performed using Kohn−Sham density functional theory (DFT) in conjunction with the Coulomb attenuated B3LYP (CAM-B3LYP)[61] exchange correlation functional. While *p*-HTAA is not a system that suggests the need for long-range corrections in the functional, this work is part of a long-term study of a large set of LCOs for which we adopt one common level of theory, and for several of the longer species these corrections are likely to be important.

For a purely QM system, the energy and strength of the vertical transition from the ground electronic state $|0\rangle$ to the excited state $|n\rangle$ are equal to those of the corresponding transition in the opposite direction. As such, an emission spectrum from state $|n\rangle$ to the ground state $|0\rangle$ for a certain molecular structure can easily be calculated as the absorption spectrum from the ground state $|0\rangle$ to the excited state $|n\rangle$ for the same structure. For the QM/MM implementation used,

dx.doi.org/10.1021/jp5009835 | J. Phys. Chem. A 2014, 118, 3419−3428

this is not true when performing calculations containing polarizabilities in the MM region. For such a case, there is a mutual relaxation of the QM and MM regions, resulting in an altered ground state wave function in the QM region and induced dipole moments in the MM region. The same relaxation does not occur for the calculation of the excited states, instead retaining the ground state induced dipole moments. As such, an asymmetry is introduced when calculating the absorption spectrum as compared to the fluorescence spectrum for a certain geometry. While other methods[62] allow relaxation to occur in both the ground and excited states, our chosen implementation does not. To avoid this problem, we have chosen to scale back the description of the MM region for all fluorescence calculations by neglecting the atomic polarizabilities and describing the solvent solely by point charges.

While the ground state conformational space of *p*-HTAA can easily be sampled from MD trajectories generated from a single starting conformation, greater care must be taken when sampling excited states. As discussed in our previous work,[38] the first electronically excited state of singlet symmetry for *p*-HTAA is to a large degree localized to the middle three thiophene rings. The excitation raises the torsional barrier between the rings to 16 kcal/mol, causing the molecule to become planar and rigid, making it highly unlikely that the barrier will be crossed at room temperature. In the previous work, this was accounted for by running separate excited state MD simulations for each ground state sample, starting from the sampled coordinates and velocities and running for a time corresponding to the fluorescence lifetime. In this work we simplify this approach by running a single excited state MD simulation for each possible starting conformation and then obtaining samples in proportion to the conformational distribution found in the ground state. For the middle three thiophene rings of *p*-HTAA, this means a total of three excited state MD simulations: *cis*−*cis*, *cis*−*trans*, and *trans*−*trans*, where *cis* indicates a dihedral angle between 0° and 90° between the sulfur atoms of two thiophene rings and *trans* indicates an angle between 90° and 180°.

III. COMPUTATIONAL DETAILS

The modifications made to the force field equilibrium bond lengths and angles were derived by fits to a zero temperature optimized geometry, obtained using the Gaussian program.[63] The calculation was performed using the B3LYP exchange-correlation fuctional[64] and the aug-cc-pVTZ[65,66] basis set.

The molecular dynamics simulations used in this work were performed using the CHARMM force field as implemented in the Tinker program.[67] The parameters used were taken from the CHARMM22 set,[68] with the exception of those previously reparametrized by us[38] and those reparameterized in this work (see Table 1), as well as the atomic charges, which were taken from the PCFF force field.[69,70] The excited state dynamics use a parametrization previously created specifically for the *p*-HTAA chromophore.[60] All MD simulations were performed in the canonical ensemble at a temperature of 300 K using the Berendsen thermostat[71] and an integration step of 1 fs. All simulations were carried out for a single solute molecule along with two sodium counterions, dissolved in a periodic box filled with water. Solvation of the chromophore was done by placing it in a box of thermally equilibrated water molecules at a concentration of 1.0 g/cm^3, removing any water molecules that overlapped with the chromophore.

Table 1. Modified CHARMM Force Field Parameters[a]

bond type	K_b	b_0
C5R-S5R	350.0	1.740
C5R-C5RP	450.0	1.375
C5RP-S5R	350.0	1.760
C5RC-C5RP	450.0	1.370
angle type	K_θ	θ_0
S5R-C5RP-C5RP	70.0	120.0
C5RP-S5R-C5RP	70.0	92.0

[a]Equilibrium bond lengths and angles have been replaced, while force constants are unaltered. K_b is given in kcal/mol/Å^2, b_0 in Å, K_θ in kcal/mol/rad^2, and θ_0 in degrees. Atom type definitions are shown in Figure 1.

The structural snapshots used for the averaged spectrum calculations were taken from MD simulations carried out in a cubic box with a side length of 34.1 Å, containing a single *p*-HTAA chromophore and 1313 water molecules. An initial MD simulation was run for 100 ps, at which point a structural snapshot was saved every 20 ps for a further 100 ps. Each of the resulting six snapshots was then used as a starting point for a separate 500 ps MD simulation, from which samples were obtained after the initial equilibration time of 100 ps.

The snapshots used for the calculation of the electric field caused by the surrounding water molecules were taken from an MD simulation of a highly symmetrical *p*-HTAA molecule held completely rigid in the center of a 34.1 × 52.7 × 40.3 Å^3 box filled with water. The sodium ions were held rigid at a large separation from the chromophore. The system was equilibrated for 50 ps, followed by another dynamic of 50 ps from which five snapshots were obtained by sampling the simulation every 10 ps.

All quantum chemical response calculations were carried out with use of the Dalton program[72,73] employing Kohn−Sham density functional theory (DFT) in conjunction with the Coulomb attenuated B3LYP (CAM-B3LYP)[61] exchange correlation functional. For the chromophore, the aug-cc-pVDZ[65,66] basis set was used in all calculations, while, for the surrounding water, the 6-31G[74] basis set was used when they were part of the QM region, and the polarizable MM potential of Ahlström et al.[75] was used when they were part of the MM region. The sodium ions were described using +1 point charges. For the line-shape function in eq 5, a unit amplitude Gaussian was employed, using a half-width half-maximum (HWHM) line broadening of 0.1 eV. This corresponds to a broadening of 13 nm in the spectral region around 400 and 20 nm in the region around 500 nm, which is broad enough to provide good spectral profiles for the adopted number of snapshots while being narrow enough to maintain all visible features of the experimental spectra.

IV. RESULTS AND DISCUSSION

A. QM/MM Study. Figure 3 shows the results of the solvation study performed on the *p*-HTAA chromophore in water. The wavelength of the dominant first excited state is plotted as a function of the thickness of the surrounding shell of water molecules. No points are included for shells of thickness 1 and 2 Å as no water molecules were within these distances. The result from the benchmark calculation is shown as a horizontal dashed line at 401 nm. This can be compared to the situation where the water solvent is completely neglected (zero shell thickness in the figure) and in which case a wavelength of

dx.doi.org/10.1021/jp5009835 | J. Phys. Chem. A 2014, 118, 3419−3428

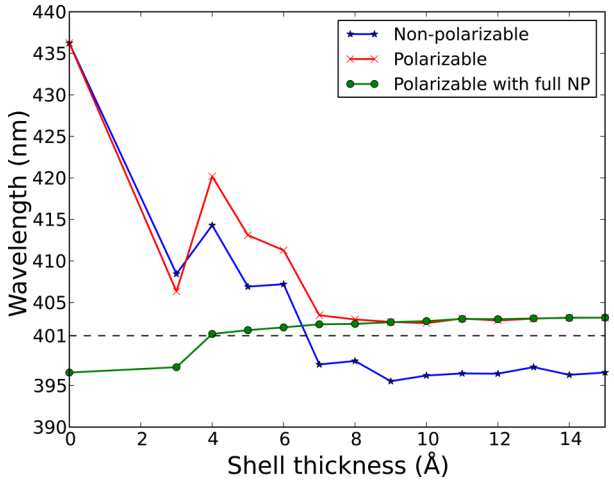

Figure 3. Transition wavelengths for the dominant excitation in a snapshot of *p*-HTAA plotted as a function of the thickness of the included layers of polarizable and nonpolarizable MM water. The dashed line at 401 nm represents the transition wavelength obtained in the benchmark calculation including a layer of QM water.

436 nm is found. This blue-shift of 35 nm, or 0.25 eV, caused by the removal of the solvent shows that the solvent has a strong influence on the absorption spectrum of the chromophore.

Adding layers of nonpolarizable water, as depicted by the blue line in Figure 3, causes a red-shift of the excitation, and the transition wavelength converges at 397 nm after 10 Å of water has been added. This result amounts to a red-shift by 4 nm, or 31 meV, compared to the reference calculation, which is a significant improvement compared to the calculation without water, and it comes at a very low additional computational cost. For this snapshot, the addition of a 15 Å shell of nonpolarizable water increases the computational time by 5% as compared to the calculation without water. The plot shows a dip for the 3 Å shell that does not fit with the trend of the rest of the curve. This can be explained by the fact that there are only 19 water molecules within this distance, and they are unevenly spread around the chromophore, not forming a full solvation shell, causing the irregularity in the trend.

Adding polarizable water in the same way produces the red curve in Figure 3. This curve converges at 403 nm, further reducing the difference to the reference calculation to a blue-shift of just 2 nm, or 1.5 meV. The convergence is both quicker, occurring at 9 Å, and smoother, with the exception of the calculation at 3 Å, compared to the curve for the nonpolarizable water description. However, this increase in quality comes at a considerable cost, with the computational time increasing by a factor of 3.9 for a 15 Å layer of polarizable water as compared to the calculation without water.

Since the computational cost of adding nonpolarizable water to the system is close to negligible, there is little reason not to include a full 15 Å shell in the solvent model. Starting from this description, it is then possible to replace some of the water molecules, beginning with those closest to the solute, with polarizable water. Performing absorption calculations for an increasing size of this polarizable layer results in the green curve in Figure 3. It should be noted here that the 0 Å point on this curve is the exact same point as the 15 Å point on the nonpolarizable curve and that the 15 Å point is the exact same point as the 15 Å point on the polarizable curve. The curve converges at approximately the same point as for the polarizable water, 9 Å. However, it comes much closer much quicker, with a good agreement found already when the polarizable shell is 4 Å thick.

At this point it is possible to continue the investigation by including an increasing layer of water in the QM region, but the high quality of the description achieved using only MM water as well as the significant computational cost of increasing the size of the QM region means that there is little to be gained by doing this.

On the basis of this study, it is now possible to identify a QM/MM model for including solvent effects in averaged spectrum calculations. Including a 5 Å thick layer of polarizable MM water molecules as well as a further 10 Å of nonpolarizable MM water includes the effects caused by the solvent to high degree while adding little to the overall computational time. For the snapshot used in this study, the excitation wavelength is red-shifted by 1 nm, or 7.7 meV, and the increase in computational time for this model as compared to neglecting the solvent entirely was by a factor of 1.3. This model will be referred to as the QM/MM(0,5,10) model.

In addition, we identify two additional models. First, a higher quality model which will be used to verify the results obtained from the QM/MM(0,5,10) model. This model includes a 9 Å thick layer of polarizable water and an additional 6 Å layer of nonpolarizable water and will be referred to as the QM/MM(0,9,6) model. This produces reliably converged results but comes at a computational cost that is 2.0 times that of the calculation without solvent. Second, a model that includes only a 15 Å layer of nonpolarizable water, referred to as the QM/MM(0,0,15) model, which is used for fluorescence spectrum calculations. These models, as well as the computational results, are summarized in Table 2.

Table 2. Comparison of the Wavelength and Oscillator Strength of the Dominant Excited State, As Well As Required Computational Time, for a Single *p*-HTAA Spectrum Calculation Using Different Models[a]

	layer thickness (Å)					
model	QM	P	NP	λ (nm)	f	time[b]
solvent neglected	0	0	0	436	0.87	1
ref	4	11	0	401	1.35	28.68
QM/MM(0,5,10) model	0	5	10	402	1.40	1.30
QM/MM(0,9,6) model	0	9	6	403	1.43	1.97
QM/MM(0,0,15) model	0	0	15	397	1.33	1.05
cut-down model	0	0	0	395	1.41	0.56

[a]The models are defined by the thickness of the solvent layers described using quantum mechanics (QM), polarizable molecular mechanics (P) and non-polarizable molecular mechanics (NP). [b]Normalized with respect to the calculation in which the solvent is neglected.

B. Solvent–Ion Cancellation. As shown by the study in the previous section, excitation energies differ significantly between absorption calculations performed on the *p*-HTAA chromophore with and without water, with a difference of 0.25 eV found for the dominant excited state. The exciton is, however, to a large degree localized within the conjugated backbone of the three middle thiophene rings. The carboxylate ion groups attached to two of these rings do not actively participate in the excitation, but their high negative charge and proximity to the rest of the system may cause a polarization of

dx.doi.org/10.1021/jp5009835 | J. Phys. Chem. A 2014, 118, 3419–3428

the parts of the system in which the exciton is formed. A simple way to approximate the electric field caused by just the carboxylate ions is to let each ion be represented by a single −0.5*e* point charge, located at the site of the oxygen. This was done for a C_{2v}-symmetrical conformation of *p*-HTAA, with all thiophene rings in trans position as shown in Figure 1. The electric field strength caused by the ions at the site of the closest carbon−carbon bond in the conjugated backbone is 0.0255 au, and for the same bonds in the middle and outer ring the field strength is 0.0092 au and 0.0065 au, respectively, as shown in Figure 4.

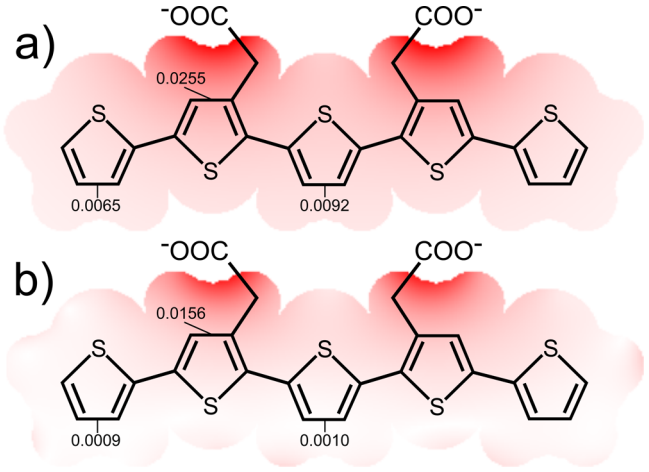

Figure 4. The electric field strength in the area of the thiophene rings of the *p*-HTAA chromophore. The upper panel (a) shows the field caused solely by the carboxylate ion groups, while the lower panel (b) shows the field of the carboxylate ion groups as well as the polarizable water surrounding the molecule. Field strengths are given in a.u.

It is of interest to see how the effect of the ions changes when water is added to the calculation. To do this, a molecular dynamics simulation was run for the rigid C_{2v}-symmetrical conformation of *p*-HTAA immersed in water, from which a number of snapshots were collected. A QM/MM calculation of the ground state energy was performed for each snapshot, employing the QM/MM solvent model from section IVA. The induced dipoles and point charges of the water molecules were then used to calculate the electric field caused by the polarized water in each snapshot, which could be averaged to obtain the field caused, on average, by the presence of the water. This field, added to that already calculated for the carboxylate ions, gives the total electric field strength in the area of the chromophore for the solvated system. In this case, the carbon−carbon bond closest to the ions experiences a field of strength 0.0156 au, which is a significant reduction compared to the unsolvated system. The field strengths for the middle and outer bonds are also greatly reduced to 0.0010 au and 0.0009 au, respectively. On the basis of these results, we conclude that the primary electronic effect of the solvent is to negate the influence of carboxylate ions.

In our previous work,[38] all spectral response calculations for *p*-HTAA were performed on a cut down version of the molecule, with the solvent entirely neglected. The cut down model, shown in Figure 1, replaces the carboxylate ion groups with hydrogens, turning the substituents on rings 2 and 4 into methyl groups. On the basis of the preceding discussion on electric field strengths, this model would appear to be a good way of giving a rough approximation of the solvent effects. This cut-down model is also appealing due to its greatly reduced computational cost. Not only is there no need to include any explicit solvent molecules, but also the size and complexity of the QM system are reduced due to the removal of the ionic groups (replacing four oxygen atoms and two carbon atoms with just two hydrogen atoms)—this model reduces the computational time by almost a factor of 2, as compared to the full *p*-HTAA chromophore without any solvent. The wavelength for the dominant excited state is found to be 395 nm, blue-shifted by 6 nm from the reference calculation.

C. Spectrum Calculations. *1. Absorption.* In order to better test accuracy of the models described in the preceding sections, an averaged room temperature absorption spectrum was calculated for the *p*-HTAA chromophore in water using each of the models. All absorption spectra for the QM/MM(0,5,10) and QM/MM(0,9,6) models as well as the cut-down model were based on the same MD simulation and the same 300 sampled structures (see the Supporting Information for an illustration of spectral convergence). Since the same structures are used in the calculations for each of the three models, not only can the resulting averaged spectrum be compared but also the differences in individual sample calculations can be addressed. Table 3 shows the mean

Table 3. Difference in Wavelengths (nm) and Percentage Change of Oscillator Strengths of the QM/MM(0,5,10) and Cut-Down Model As Compared to the QM/MM(0,9,6) Model, Averaged over 300 Snapshot Calculations, along with the Standard Deviations

model	$\Delta\lambda$	$\sigma\lambda$	Δf	σf
QM/MM(0,5,10) model	−2.00	1.56	−2.08	1.40
cut-down model	−8.25	4.62	−4.79	6.85

difference in wavelength and percentage change in oscillator strength of the dominant first excitation, as well as their standard deviations, when comparing individual calculations for the QM/MM(0,5,10) and cut-down models to those of the reference QM/MM(0,9,6) model. This shows that in the case of the QM/MM(0,5,10) model, the small blue-shift of 2.0 nm is quite systematic, with only a low standard deviation of 1.6 nm. The same is true for the cut-down model, though with a larger blue-shift of 8.3 nm and a larger, though still small, standard deviation of 4.6 nm. The differences in oscillator strengths follow the same pattern, with a somewhat larger difference and standard deviation for the cut-down model as compared to the QM/MM(0,5,10) model. However, the differences in both cases are small, representing only a 2% change in strength for the QM/MM(0,5,10) model and a 5% change in the case of the cut-down model, as compared to the average oscillator strength of the QM/MM(0,9,6) model calculations.

The resulting averaged spectra for the three models are shown in Figure 5 alongside an experimentally obtained spectrum. The QM/MM(0,9,6) spectrum shows an excellent agreement with experimental results, both in the position of the peak of the main absorption band, which is red-shifted by just 2 nm compared to the experimental peak found at 393 nm, as well as in the spectral profile, which has an asymmetrical broadening with a more triangular shape for the high energy side. The spectrum obtained with the QM/MM(0,5,10) model is in similarly excellent agreement with the experimental spectrum, with a peak that is in perfect agreement with the

dx.doi.org/10.1021/jp5009835 | J. Phys. Chem. A 2014, 118, 3419−3428

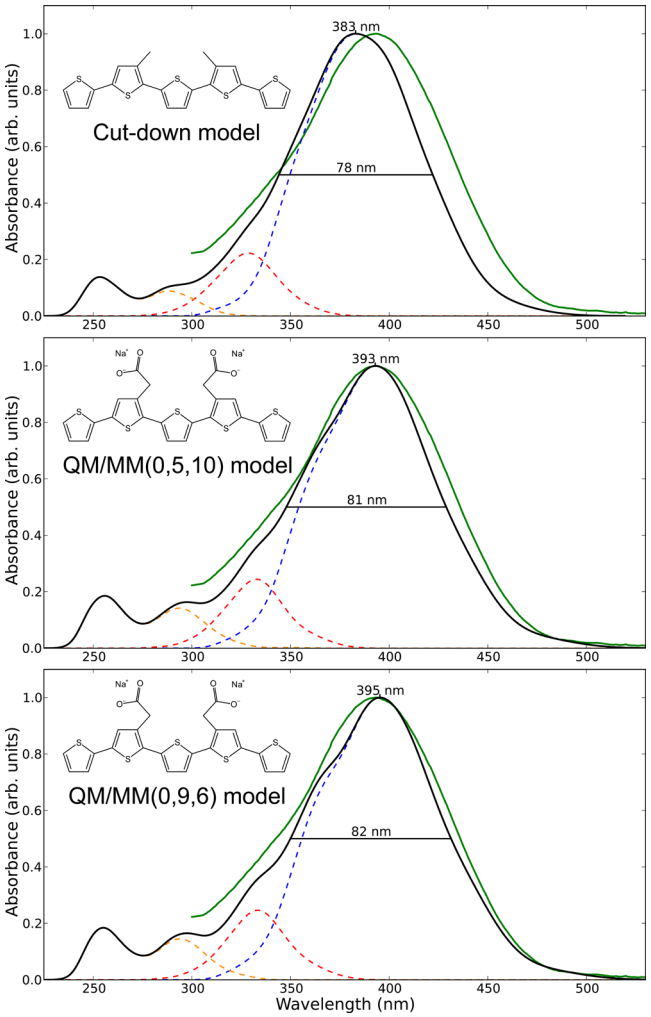

Figure 5. Theoretical room temperature absorption spectra for *p*-HTAA, based on 300 snapshots, including the 10 lowest excited states. Dashed lines indicate the contributions from the first, second, and remaining eight excited states. Experimental spectrum[38] is included in green.

experimental peak, although the general position of the band is slightly blue-shifted as compared to that of the experimental spectrum and that of the QM/MM(0,9,6) model. The cut-down model shows a more significant difference to the QM/MM(0,9,6) model, with a peak that is red-shifted by 10 nm compared to the experimental peak as well as a less apparent asymmetrical broadening.

The difference in the shape of the spectral band between the cut-down model and the QM/MM models has been investigated by studying the structure, excitation wavelengths, and oscillator strengths of the individual snapshots used for the spectra. This showed that for snapshots that have longer excitation wavelength, the difference between the QM/MM and cut-down models is larger. In addition, an inverse correlation was found between the difference in wavelength between the models and the difference in oscillator strength. That is, a snapshot that shows a large difference in excitation wavelength between the models is likely not to show a large difference in oscillator strength, and vice versa. This is consistent with the change seen in the spectral profiles, but does not explain the reason for it. A number of structural parameters were studied alongside the shifts in wavelength and oscillator strength, though no clear correlation has been found, leading us to believe that it is a complex combination of many factors leading to the changes in the spectrum. A full description of the studied parameters can be found in the Supporting Information.

2. Fluorescence. From the structural snapshots sampled from the ground state MD trajectory, a distribution of conformations was found for the middle three thiophene rings of *p*-HTAA, with 28% found in the *cis*−*cis* conformation, 50% in the *cis*−*trans* conformation, and 22% in the *trans*−*trans* conformation. On the basis of this, a proportional sampling of excited state MD simulations started in each of the three conformations was obtained, resulting in 300 excited state snapshots. These were then used for averaged fluorescence spectrum calculations, performed using the QM/MM(0,0,15) model as well as the cut-down model. These are shown, along with an experimentally obtained fluorescence spectrum, in Figure 6. The resulting spectral bands are close to identical,

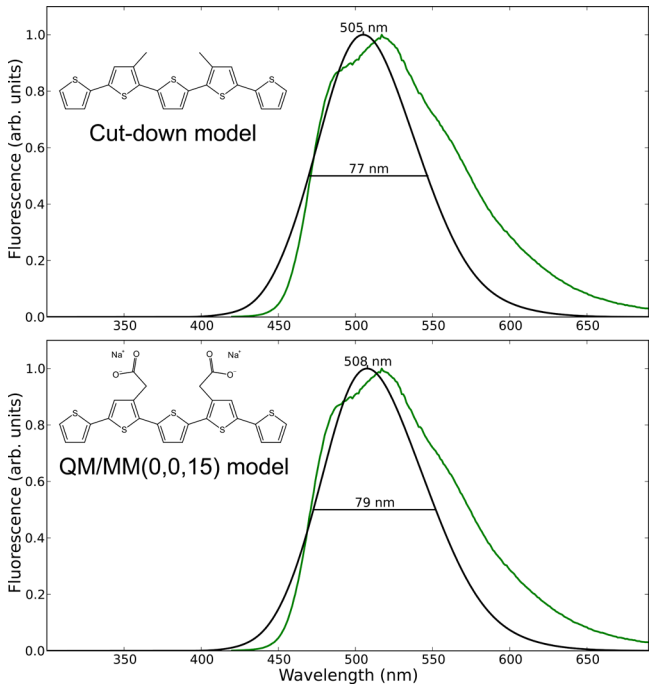

Figure 6. Theoretical room temperature fluorescence spectra for *p*-HTAA based on 300 snapshots. Experimental spectrum[38] is included in green.

with the only difference being a blue-shift of 3 nm for the spectrum obtained using the cut-down model as well as a slight narrowing of the band by 2 nm. Due to the presence of a vibrational progression in the experimental fluorescence spectrum, the peak found at 517 nm is somewhat unrepresentative of the position of the emission band. This taken into consideration, the theoretical peaks at 508 and 505 nm for the QM/MM(0,0,15) model and cut-down model, respectively, compare well to the experimental peak. Though somewhat narrower than the experimental emission band, the theoretical bands show an excellent agreement in both the position and the shape of the band, exhibiting a slope that is steeper on the high energy side than on the low energy side.

dx.doi.org/10.1021/jp5009835 | J. Phys. Chem. A 2014, 118, 3419−3428

V. CONCLUSIONS

A QM/MM−MD model has been developed for the inclusion of solvent effects when performing calculations of luminescence properties of conjugated polyelectrolytes, and we exemplify the use of this model by a study of absorption/excitation and fluorescence spectra of conjugated oligothiophenes.

The model divides the system into a region described using quantum mechanics, containing the solute, a 5 Å thick shell of water described at the polarizable level, and a 10 Å thick layer of water described at the nonpolarizable level. The model has been tuned to include the effect of the solvent to a large degree while also not significantly increasing the computational cost of the calculation. For the test case studied in the present work, the solvent model results in a transition energy that is blue-shifted by 1 nm, or 7.7 meV, compared to a high quality reference calculation, while only increasing the computational time of the calculation by a factor of 1.3 as compared to the same calculation without solvent.

It is demonstrated that the effect of the polar water solvent largely diminishes the polarization of electrons in the conjugated backbone due to the negative carboxylate ions. This leads to a simple and computationally cost efficient model system in which the carboxylate ions are replaced neutral hydrogen atoms. For the studied test case, this approximation leads to a blue-shift of 6 nm, or 47 meV, compared to the reference calculation, and a reduction in computational time (compared to the calculation without water) of 46%.

When compared against benchmark experimental absorption and fluorescence spectra, the best theoretical results are shown to be quantitatively accurate. This observed high quality includes not only band maxima but also intensities and profiles. The accurate description of the asymmetrical broadening in the absorption spectrum is shown to require a combination of a well converged sampling of the chromophore conformational space and an accurate account of the solvent in the response calculations.

■ ASSOCIATED CONTENT

Ⓢ Supporting Information

An investigation of the spectral convergence for increasing sample size is provided as well as a study of the correlation between structural and spectral properties of the samples. This material is available free of charge via the Internet at http://pubs.acs.org.

■ AUTHOR INFORMATION

Corresponding Author

*Phone: +46-13281688; e-mail: panor@ifm.liu.se.

Notes

The authors declare no competing financial interest.

■ ACKNOWLEDGMENTS

We acknowledge financial support from the Swedish Research Council (Grant No. 621-2010-5014) as well as a grant for computing time at National Supercomputer Centre (NSC), Sweden. M.L. thanks the Swedish e-Science Research Center (SeRC) for financial support.

■ REFERENCES

(1) Nilsson, K. P. R.; Hammarström, P.; Ahlgren, F.; Herland, A.; Schnell, E. A.; Lindgren, M.; Westermark, G. T.; Ingänas, O. Conjugated Polyelectrolytes - Conformation-Sensitive Optical Probes for Staining and Characterization of Amyloid Deposits. *ChemBioChem* **2006**, *7*, 1096−1104.

(2) Bacskai, B. J.; Hickey, G. A.; Skoch, J.; Kajdasz, S. T.; Wang, Y.; Huang, G.-F.; Mathis, C. A.; Klunk, W. E.; Hyman, B. T. Four-Dimensional Multiphoton Imaging of Brain Entry, Amyloid Binding, and Clearance of an Amyloid-Beta Ligand in Transgenic Mice. *Proc. Natl. Acad. Sci. U.S.A.* **2003**, *100*, 12462−12467.

(3) Klunk, W. E.; Bacskai, B. J.; Mathis, C. A.; Kajdasz, S. T.; McLellan, M. E.; Frosch, M. P.; Debnath, M. L.; Holt, D. P.; Wang, Y.; Hyman, B. T. Imaging Aβ Plaques in Living Transgenic Mice With Multiphoton Microscopy and Methoxy-X04, a Systemically Administered Congo Red Derivative. *J. Neuropathol. Exp. Neurol.* **2002**, 797−805.

(4) Reinke, A. A.; Gestwicki, J. E. Insight into Amyloid Structure Using Chemical Probes. *Chem. Biol. Drug. Des.* **2011**, *77*, 399−411.

(5) Cui, M.; Li, Z.; Tang, R.; Jia, H.; Liu, B. Novel (*E*)-5-styryl-2,2′-Bithiophene Derivatives as Ligands for β-Amyloid Plaques. *Eur. J. Med. Chem.* **2011**, *46*, 2908−2916.

(6) Buell, A. K.; Esbjörner, E. K.; Riss, P. J.; White, D. A.; Aigbirhio, F. I.; Toth, G.; Welland, M. E.; Dobson, C. M.; Knowles, T. P. J. Probing Small Molecule Binding to Amyloid Fibrils. *Phys. Chem. Chem. Phys.* **2011**, *13*, 20044−20052.

(7) Okamura, N.; Suemoto, T.; Shimadzu, H.; Suzuki, M.; Shiomitsu, T.; Akatsu, H.; Yamamoto, T.; Staufenbiel, M.; Yanai, K.; Arai, H.; et al. Styrylbenzoxazole Derivatives for *in Vivo* Imaging of Amyloid Plaques in the Brain. *J. Neurosci.* **2004**, *24*, 2535−2541.

(8) Mathis, C. A.; Bacskai, B. J.; Kajdasz, S. T.; McLellan, M. E.; Frosch, M. P.; Hyman, B. T.; Holt, D. P.; Wang, Y.; Huang, G.-F.; Debnath, M. L.; Klunk, W. E. A Lipophilic Thioflavin-T Derivative for Positron Emission Tomography (PET) Imaging of Amyloid in Brain. *Bioorg. Med. Chem. Lett.* **2002**, *12*, 295−298.

(9) Klunk, W. E.; Engler, H.; Nordberg, A.; Wang, Y.; Blomqvist, G.; Holt, D. P.; Bergström, M.; Savitcheva, I.; Debnath, M. L.; Barletta, J.; et al. Imaging Brain Amyloid in Alzheimer's Disease with Pittsburgh Compound-B. *Ann. Neurol.* **2004**, *55*, 306−319.

(10) Nesterov, E. E.; Skoch, J.; Hyman, B. T.; Klunk, W. E.; Bacskai, B. J.; Swager, T. M. *in Vivo* Optical Imaging of Amyloid Aggregates in Brain: Design of Fluorescent Markers. *Angew. Chem., Int. Ed.* **2005**, *44*, 5452−5456.

(11) Kung, M.-P.; Hou, C.; Zhuang, Z.-P.; Skovronsky, D. M.; Zhang, B.; Gur, T. L.; Trojanowski, J. Q.; Lee, V. M. Y.; Kung, H. F. Radioiodinated Styrylbenzene Derivatives as Potential SPECT Imaging Agents for Amyloid Plaque Detection in Alzheimer's Disease. *J. Mol. Neurosci.* **2002**, *19*, 7−10.

(12) Kim, I.-B.; Shin, H.; Garcia, A. J.; Bunz, U. H. F. Use of a Folate-PPE Conjugate to Image Cancer Cells *in Vitro*. *Bioconjugate Chem.* **2007**, *18*, 815−820.

(13) Moon, J. H.; MacLean, P.; McDaniel, W.; Hancock, L. F. Conjugated Polymer Nanoparticles for Biochemical Protein Kinase Assay. *Chem. Commun.* **2007**, 4910−4912.

(14) Bryson, J. M.; Fichter, K. M.; Chu, W.-J.; Lee, J.-H.; Li, J.; Madsen, L. A.; McLendon, P. M.; Reineke, T. M. Polymer Beacons for Luminescence and Magnetic Resonance Imaging of DNA Delivery. *Proc. Natl. Acad. Sci. U.S.A.* **2009**, *106*, 16913−16918.

(15) Domaille, D. W.; Que, E. L.; Chang, C. J. Synthetic Fluorescent Sensors for Studying the Cell Biology of Metals. *Nat. Chem. Biol.* **2008**, *4*, 168−175.

(16) Björk, P.; Nilsson, K. P. R.; Lenner, L.; Kågedal, B.; Persson, B.; Inganäs, O.; Jonasson, J. Conjugated Polythiophene Probes Target Lysosome-Related Acidic Vacuoles in Cultured Primary Cells. *Mol. Cell. Probes* **2007**, *21*, 329−337.

(17) Pu, K.-Y.; Shi, J.; Cai, L.; Li, K.; Liu, B. Affibody-Attached Hyperbranched Conjugated Polyelectrolyte for Targeted Fluorescence Imaging of HER2-Positive Cancer Cell. *Biomacromolecules* **2011**, *12*, 2966−2974.

(18) McRae, R. L.; Phillips, R. L.; Kim, I.-B.; Bunz, U. H. F.; Fahrni, C. J. Molecular Recognition Based on Low-Affinity Polyvalent Interactions: Selective Binding of a Carboxylated Polymer to

Fibronectin Fibrils of Live Fibroblast Cells. *J. Am. Chem. Soc.* **2008**, *130*, 7851−7853.
(19) Liu, J.; Ding, D.; Geng, J.; Liu, B. PEGylated Conjugated Polyelectrolytes Containing 2,1,3-Benzoxadiazole Units for Targeted Cell Imaging. *Polym. Chem.* **2012**, *3*, 1567−1575.
(20) Li, K.; Pu, K.-Y.; Cai, L.; Liu, B. Phalloidin-Functionalized Hyperbranched Conjugated Polyelectrolyte for Filamentous Actin Imaging in Living Hela Cells. *Chem. Mater.* **2011**, *23*, 2113−2119.
(21) Zhang, J.; Campbell, R. E.; Ting, A. Y.; Tsien, R. Y. Creating New Fluorescent Probes for Cell Biology. *Nat. Rev. Mol. Cell Biol.* **2002**, *3*, 906−918.
(22) Michalet, X.; Pinaud, F. F.; Bentolila, L. A.; Tsay, J. M.; Doose, S.; Li, J. J.; Sundaresan, G.; Wu, A. M.; Gambhir, S. S.; Weiss, S. Quantum Dots for Live Cells, *in Vivo* Imaging, and Diagnostics. *Science* **2005**, *307*, 538−544.
(23) Resch-Genger, U.; Grabolle, M. Quantum Dots Versus Organic Dyes as Fluorescent Labels. *Nat. Methods* **2008**, *5*, 763−775.
(24) Frangioni, J. *In Vivo* Near-Infrared Fluorescence Imaging. *Curr. Opin. Chem. Biol.* **2003**, *7*, 626−634.
(25) Feng, G.; Ding, D.; Liu, B. Fluorescence Bioimaging with Conjugated Polyelectrolytes. *Nanoscale* **2012**, *4*, 6150−6165.
(26) Pu, K.-Y.; Liu, B. Fluorescent Conjugated Polyelectrolytes for Bioimaging. *Adv. Funct. Mater.* **2011**, *21*, 3408−3423.
(27) Duarte, A.; Pu, K.-Y.; Liu, B.; Bazan, G. C. Recent Advances in Conjugated Polyelectrolytes for Emerging Optoelectronic Applications. *Chem. Mater.* **2011**, *23*, 501−515.
(28) Hoven, C. V.; Garcia, A.; Bazan, G. C.; Nguyen, T.-Q. Recent Applications of Conjugated Polyelectrolytes in Optoelectronic Devices. *Adv. Mater.* **2008**, *20*, 3793−3810.
(29) Taranekar, P.; Qiao, Q.; Jiang, H.; Ghiviriga, I.; Schanze, K. S.; Reynolds, J. R. Hyperbranched Conjugated Polyelectrolyte Bilayers for Solar-Cell Applications. *J. Am. Chem. Soc.* **2007**, *129*, 8958−8959.
(30) Liu, X.; Zhu, R.; Zhang, Y.; Liu, B.; Ramakrishna, S. Anionic Benzothiadiazole Containing Polyfluorene and Oligofluorene as Organic Sensitizers for Dye-Sensitized Solar Cells. *Chem. Commun.* **2008**, 3789−3791.
(31) Thomas, S. W.; Joly, G. D.; Swager, T. M. Chemical Sensors Based on Amplifying Fluorescent Conjugated Polymers. *Chem. Rev.* **2007**, *107*, 1339−1386.
(32) Lee, K.; Povlich, L. K.; Kim, J. Recent Advances in Fluorescent and Colorimetric Conjugated Polymer-Based Biosensors. *Analyst* **2010**, *135*, 2179−2189.
(33) Feng, X.; Liu, L.; Wang, S.; Zhu, D. Water-soluble Fluorescent Conjugated Polymers and Their Interactions with Biomacromolecules for Sensitive Biosensors. *Chem. Soc. Rev.* **2010**, *39*, 2411−2419.
(34) Åslund, A.; Sigurdson, C. J.; Klingstedt, T.; Grathwohl, S.; Bolmont, T.; Dickstein, D. L.; Glimsdal, E.; Prokop, S.; Lindgren, M.; Konradsson, P.; et al. Novel Pentameric Thiophene Derivatives for *in Vitro* and *in Vivo* Optical Imaging of a Plethora of Protein Aggregates in Cerebral Amyloidoses. *ACS Chem. Biol.* **2009**, *4*, 673−684.
(35) Klingstedt, T.; Nilsson, K. P. R. Luminescent Conjugated Poly- and Oligothiophenes: Optical Ligands for Spectral Assigment of a Plethora of Protein Aggregates. *Biochem. Soc. Trans.* **2012**, *40*, 704−710.
(36) Nilsson, K. P. R.; Åslund, A.; Berg, I.; Nyström, S.; Konradsson, P.; Herland, A.; Inganäs, O.; Stabo-Eeg, F.; Lindgren, M.; Westermark, G. T.; et al. Imaging Distinct Conformational States of Amyloid-Beta Fibrils in Alzheimer's Disease Using Novel Luminescent Probes. *ACS Chem. Biol.* **2007**, *2*, 553−560.
(37) Klingstedt, T.; Åslund, A.; Simon, R. S.; Johansson, L. B. G.; Mason, J. J.; Nyström, S.; Hammarström, P.; Nilsson, K. P. R. Synthesis of a Library of Oligothiophenes and Their Utilization as Fluorescent Ligands for Spectral Assigment of Protein Aggregates. *Org. Biomol. Chem.* **2011**, *9*, 8356−8370.
(38) Sjöqvist, J.; Linares, M.; Lindgren, M.; Norman, P. Molecular Dynamics Effects on Luminescence Properties of Oligothiophene Derivatives: A Molecular Mechanics−Response Theory Study Based on the CHARMM Force Field and Density Functional Theory. *Phys. Chem. Chem. Phys.* **2011**, *13*, 17532−17542.
(39) Tomasi, J.; Maurizio, P. Molecular Interactions in Solution: An Overview of Methods Based on Continuous Distributions of the Solvent. *Chem. Rev.* **1994**, *94*, 2027−2094.
(40) Cramer, R.; Truhlar, D. G. Implicit solvation models: Equilibria, structure, spectra, and dynamics. *Chem. Rev.* **1999**, *99*, 2161−2200.
(41) Tomasi, J.; Mennucci, B.; Cammi, R. Quantum Mechanical Continuum Solvation Models. *Chem. Rev.* **2005**, *105*, 2999−3093.
(42) Mikkelsen, K. V. Correlated Electronic Structure Nonlinear Response Methods for Structured Environments. *Annu. Rev. Phys. Chem.* **2006**, *57*, 365−402.
(43) Kongsted, J.; Osted, A.; Mikkelsen, K. V.; Christiansen, O. Coupled Cluster/Molecular Mechanics Method: Implementation and Application to Liquid Water. *J. Phys. Chem. A* **2003**, *107*, 2578−2588.
(44) Kongsted, J.; Osted, A.; Mikkelsen, K. V.; Christiansen, O. Linear Response Functions for Coupled Cluster/Molecule Mechanics Including Polarization Interactions. *J. Chem. Phys.* **2003**, *118*, 1620−1633.
(45) Kongsted, J.; Osted, A.; Mikkelsen, K. V.; Christiansen, O. Nonlinear Optical Response Properties of Molecules in Condensed Phases Using the Coupled Cluster/Dielectric Continuum or Molecular Mechanics Methods. *J. Chem. Phys.* **2003**, *119*, 10519−10535.
(46) Kongsted, J.; Osted, A.; Mikkelsen, K. V.; Christiansen, O. Second Harmonic Generation Second Hyperpolarizability of water Calculated Using the Combined Coupled Cluster Dielectric Continuum or Different Molecular Mechanics Methods. *J. Chem. Phys.* **2004**, *120*, 3787−3798.
(47) Kongsted, J.; Osted, A.; Mikkelsen, K. V.; Christiansen, O. The QM/MM Approach for Wavefunctions, Energies and Response Functions Within Self-Consistent Field and Coupled Cluster Theories. *Mol. Phys.* **2002**, *100*, 1813−1828.
(48) Nielsen, C. B.; Christiansen, O.; Mikkelsen, K. V.; Kongsted, J. Density Functional Self-Consistent Quantum Mechanics/Molecular Mechanics Theory for Linear and Nonlinear Molecular Properties: Applications to Solvated Water and Formaldehyde. *J. Chem. Phys.* **2007**, *126*, 154112−154300.
(49) Lin, H.; Truhlar, D. G. QM/MM: What Have We Learned, Where Are We, and Where Do We Go from Here? *Theor. Chem. Acc.* **2007**, *117*, 185−199.
(50) Senn, H. M.; Thiel, W. QM/MM methods for Biomolecular Systems. *Angew. Chem. Int. Edn* **2009**, *48*, 1198−1229.
(51) Kongsted, J.; Osted, A.; Mikkelsen, K. V.; Åstrand, P.-O.; Christiansen, O. Solvent Effects on the n −> pi* Electronic Transition in Formaldehyde: A Combined Coupled Cluster/Molecular Dynamics Study. *J. Chem. Phys.* **2004**, *121*, 8435−8445.
(52) Thompson, M. A. QM/MMpol: A Consistent Model for Solute/Solvent Polarization. Application to the Aqueous Solvation and Spectroscopy of Formaldehyde, Acetaldehyde, and Acetone. *J. Phys. Chem.* **1996**, *100*, 14492−14507.
(53) Aidas, K.; Mikkelsen, K. V.; Mennucci, B.; Kongsted, J. Fluorescence and Phosphorescence of Acetone in Neat Liquid and Aqueous Solution Studied by QM/MM and PCM Approaches. *Int. J. Quantum Chem.* **2011**, *111*, 1511−1520.
(54) Parac, M.; Doerr, M.; Marian, C. M.; Thiel, W. QM/MM Calculation of Solvent Effects on Absorption Spectra Quanine. *J. Comput. Chem.* **2010**, *31*, 90−106.
(55) Poulsen, T. D.; Kongsted, J.; Osted, A.; Ogilby, P. R.; Mikkelsen, K. V. The Combined Multiconfigurational Self-Consistent-Field/Molecular Mechanics Wave Function Approach. *J. Chem. Phys.* **2001**, *115*, 2393−2400.
(56) Sanchez, M. L.; Aguilar, M. A.; Olivares del Valle, F. J. Study of Solvent Effects by Means of Averaged Solvent Electrostatic Potentials Obtained from Molecular Dynamics Data. *J. Comput. Chem.* **1997**, *18*, 313−322.
(57) Osted, A.; Kongsted, J.; Mikkelsen, K. V.; Christiansen, O. Linear Response Properties of Liquid Water Calculated Using CC2 and CCSD Within Different Molecular Mechanics Methods. *J. Phys. Chem. A* **2004**, *108*, 8646−8658.
(58) Poulsen, T. D.; Ogilby, P.; Mikkelsen, K. V. Linear Response Properties for Solvated Molecules Described by a Combined

Multiconfigurational Self-Consistent-Field/Molecular Mechanics Model. *J. Chem. Phys.* **2002**, *116*, 3730−3738.
(59) Gonzáles Cano, R. C.; Herrera, H.; Seguera, J. L.; López Navarrete, J. T.; Ruiz Delgado, M. C.; Casado, J. Conformational Control of The Electronic Properties of an *α-β* Terthiophene: Lessons from a Precursor Towards Dendritic Hyperbranched Oligo- and Polythiophenes. *ChemPhysChem* **2012**, *13*, 3893−3900.
(60) Sjöqvist, J.; Linares, M.; Norman, P. Platinum(II) and Phosphorous MM3 Force Field Parameterization for Chromophore Absorption Spectra at Room Temperature. *J. Phys. Chem. A* **2010**, *114*, 4981−4987.
(61) Yanai, T.; Tew, D. P.; Handy, N. C. A New Hybrid Exchange-Correlation Functional Using the Coulomb-Attenuating Method (CAM-B3LYP). *Chem. Phys. Lett.* **2004**, *393*, 51−57.
(62) Marenich, A. V.; Cramer, C. J.; Truhlar, D. G.; Guido, C. A.; Mennucci, B.; Scalmani, G.; Frisch, M. J. Practical Computation of Electronic Excitation in Solution: Vertical Excitation Model. *Chem. Sci.* **2011**, *2*, 2143−2161.
(63) Frisch, M. J.; Trucks, G. W.; Schlegel, H. B.; Scuseria, G. E.; Robb, M. A.; Cheeseman, J. R.; Scalmani, G.; Barone, V.; Mennucci, B.; Petersson, G. A.; et al. *Gaussian 09*, Revision A.02; Gaussian, Inc.: Wallingford, CT, 2009.
(64) Becke, A. D. Density-Functional Thermochemistry. III. The Role of Exact Exchange. *J. Chem. Phys.* **1993**, *98*, 5648−5652.
(65) Kendall, R. A.; Dunning, T. H., Jr.; Harrison, R. J. Electron Affinities of the First-Row Atoms Revisited. Systematic Basis Sets and Wave Functions. *J. Chem. Phys.* **1992**, *96*, 6796−6806.
(66) Woon, D. E.; Dunning, T. H., Jr. Gaussian-Basis Sets for Use in Correlated Molecular Calculations. 3. The Atoms Aluminum Through Argon. *J. Chem. Phys.* **1993**, *98*, 1358−1371.
(67) Ponder, J. W.; *TINKER*, Version 5.0; Washington University: Saint Louis, MO
(68) MacKerell, A. D., Jr.; Bashford, D.; Bellott, M.; Dunbrack, R. L., Jr.; Evanseck, J. D.; Field, M. J.; Fischer, S.; Gao, J.; Guo, H.; Ha, S.; et al. All-Atom Empirical Potential for Molecular Modeling and Dynamic Studies of Proteins. *J. Phys. Chem. B* **1998**, *102*, 3586−3616.
(69) Maple, J. R.; Dinur, U.; Hagler, A. T. Derivation of Force Fields for Molecular Mechanics and Dynamics from *ab Initio* Energy Surfaces. *Proc. Natl. Acad. Sci. U. S. A.* **1988**, *85*, 5350−5354.
(70) Maple, J. R.; Hwang, M. J.; Stockfisch, T. P.; Dinur, U.; Waldman, M.; Ewig, C. S.; Hagler, A. T. Derivation of Class II Force Fields. I. Methodology and Quantum Force Field for the Alkyl Functional Group and Alkane Molecules. *J. Comput. Chem.* **1994**, *15*, 162−182.
(71) Berendsen, H. J. C.; Postma, J. P. M.; van Gunsteren, W. F.; DiNola, A.; Haak, J. R. Molecular Dynamics with Coupling to an External Bath. *J. Chem. Phys.* **1984**, *81*, 3684−3690.
(72) *DALTON, A Molecular Electronic Structure Program*, Release DALTON2013.0, 2013; http://daltonprogram.org.
(73) Aidas, K.; Angeli, C.; Bak, K. L.; Bakken, V.; Bast, R.; Boman, L.; Christiansen, O.; Cimiraglia, R.; Coriani, S.; Dahle, P.; et al. The Dalton Quantum Chemistry Program System. *WIREs Comput. Mol. Sci.* **2014**, *4*, 269−284.
(74) Hehre, W. J.; Ditchfield, R.; Pople, J. A. Self-Consistent Molecular Orbital Methods. XII. Further Extensions of Gaussian-Type Basis Sets for Use in Molecular Orbital Studies of Organic Molecules. *J. Chem. Phys.* **1972**, *56*, 2257−2261.
(75) Ahlström, P.; Wallqvist, A.; Engström, S.; Jönsson, B. A Molecular Dynamics Study of Polarizable Water. *Mol. Phys.* **1989**, *68*, 563−581.